Direct membrane binding and self-interaction contribute to Mmr1 function in mitochondrial inheritance

WeiTing Chen, Holly A. Ping, and Laura L. Lackner*
Department of Molecular Biosciences, Northwestern University, Evanston, IL 60208

ABSTRACT **Mitochondrial transport and anchoring mechanisms work in concert to position mitochondria to meet cellular needs. In yeast, Mmr1 functions as a mitochondrial adaptor for Myo2 to facilitate actin-based transport of mitochondria to the bud. Posttransport, Mmr1 is proposed to anchor mitochondria at the bud tip. Although both functions require an interaction between Mmr1 and mitochondria, the molecular basis of the Mmr1–mitochondria interaction is poorly understood. Our in vitro phospholipid binding assays indicate Mmr1 can directly interact with phospholipid membranes. Through structure–function studies we identified an unpredicted membrane-binding domain composed of amino acids 76–195 that is both necessary and sufficient for Mmr1 to interact with mitochondria in vivo and liposomes in vitro. In addition, our structure–function analyses indicate that the coiled-coil domain of Mmr1 is necessary and sufficient for Mmr1 self-interaction and facilitates the polarized localization of the protein. Disrupting either the Mmr1–membrane interaction or Mmr1 self-interaction leads to defects in mitochondrial inheritance. Therefore, direct membrane binding and self-interaction are necessary for Mmr1 function in mitochondrial inheritance and are utilized as a means to spatially and temporally regulate mitochondrial positioning.**

Monitoring Editor
Thomas D. Fox
Cornell University

Received: Feb 13, 2018
Revised: Jul 9, 2018
Accepted: Jul 17, 2018

INTRODUCTION

Mitochondrial positioning is an active and regulated process that couples the distribution of the organelle with the needs of the cell. The position of mitochondria is determined in part by the activities of mitochondrial transport and anchoring (Labbe *et al.*, 2014; Lackner, 2014). Coordinated regulation of these activities ensures mitochondria are trafficked to and dynamically maintained at specific cellular locations. For example, mitochondria are positioned in specific regions of activated immune cells and axons to serve as local providers of energy and calcium buffering (Chada and Hollenbeck, 2004; Quintana *et al.*, 2007; Schwarz, 2013; Lin and Sheng, 2015). The positioning of mitochondria at the oocyte posterior in *Drosophila* is required for the efficient incorporation of mitochondria into primordial germ cells (Hurd *et al.*, 2016). In addition, in asymmetrically dividing cell types such as yeast and stem-like cells, mitochondrial positioning pathways likely influence the asymmetric age/function-dependent inheritance of mitochondria, which affects the fate of each daughter (McFaline-Figueroa *et al.*, 2011; Katajisto *et al.*, 2015; Pernice *et al.*, 2016, 2017; Kraft and Lackner, 2018). Although players in mitochondrial positioning pathways have been identified, a deeper understanding of the molecular mechanism as well as the spatial, temporal, and contextual regulation of these proteins is required to understand how mitochondria are positioned at the right place and time to meet cellular needs.

In yeast, the antagonistic functions of bud and mother cell positioning mechanisms govern the partitioning of mitochondria between the mother and daughter. Mitochondrial transport to the bud begins early in the cell cycle and is dependent on Myo2, a type V myosin that drives actin-based transport of mitochondria to the bud (Simon *et al.*, 1997; Itoh *et al.*, 2002; Altmann *et al.*, 2008; Fortsch *et al.*, 2011). Mmr1 and Ypt11 function as adaptors that

This article was published online ahead of print in MBoC in Press (http://www.molbiolcell.org/cgi/doi/10.1091/mbc.E18-02-0122) on July 25, 2018.
The authors declare no competing financial interests.
*Address correspondence to: Laura L. Lackner (Laura.Lackner@northwestern.edu).
Abbreviations used: AD, activation domain; BD, binding domain; CBD, cargo-binding domain; CC, coiled-coil; CL, cardiolipin; DDO, double-dropout; ER, endoplasmic reticulum; EV, empty vector; IP, immunoprecipitation; MECA, mitochondria–ER–cortex anchor; mitoBD, mitochondria binding domain; OMC, outer membrane composition; PA, phosphatidic acid; PC, phosphatidylcholine; PE, phosphatidylethanolamine; PG, phosphatidylglycerol; PI, phosphatidylinositol; PS, phosphatidylserine; SC, synthetic complete; TDO, triple-dropout; YPD, yeast extract peptone dextrose.

link mitochondria to Myo2, and either Mmr1 or Ypt11 is required for Myo2-dependent transport of mitochondria to buds (Itoh *et al.*, 2002, 2004; Boldogh *et al.*, 2004; Frederick *et al.*, 2008; Eves *et al.*, 2012; Chernyakov *et al.*, 2013; Lewandowska *et al.*, 2013). Mmr1 is also proposed to function in the retention of mitochondria in buds by physically tethering mitochondria to cortical endoplasmic reticulum (ER) sheets at the bud tip (Swayne *et al.*, 2011). The movement into and anchoring of mitochondria in buds are counterbalanced by two mitochondrial anchors that function to retain mitochondria in mother cells, the mitochondria–ER–cortex anchor (MECA) and Mfb1 (Cerveny *et al.*, 2007; Klecker *et al.*, 2013; Lackner *et al.*, 2013; Pernice *et al.*, 2016). How the localization and activity of these proteins are regulated in space and time to govern the distribution and inheritance of the mitochondrial network over the course of the cell cycle are poorly understood.

Mmr1 must interact with both mitochondria and Myo2 to function in mitochondrial positioning. A Myo2-binding domain within Mmr1 has been characterized and shown to be sufficient for interaction with the motor (Itoh *et al.*, 2004; Eves *et al.*, 2012). A mitochondrial binding region within Mmr1 has also been described (Itoh *et al.*, 2004). However, the molecular basis of the interaction between Mmr1 and mitochondria is undefined. In addition, the contributions of Mmr1's predicted coiled-coil domain to overall Mmr1 function are not clear (Itoh *et al.*, 2004). Here, we use a structure–function analysis of Mmr1 to gain insight into the functional contributions of various Mmr1 domains. We identified a membrane-binding domain in Mmr1 that is required for the interaction with mitochondria and Mmr1-mediated mitochondrial inheritance. In addition, our studies indicate the coiled-coil domain of Mmr1 mediates an Mmr1-Mmr1 interaction, which facilitates the polarized localization of the protein and, consequently, impacts Mmr1 function. We predict that the activities of direct membrane binding and self-interaction are regulated to spatially and temporally control Mmr1 function in the cell.

RESULTS

Mmr1 interacts directly with phospholipid membranes

Mmr1 is a soluble protein that interacts peripherally with mitochondria (Itoh *et al.*, 2004). However, the molecular basis for the Mmr1–mitochondria interaction is unknown. We have shown that Num1, the core protein component of the mitochondrial tether MECA (Lackner *et al.*, 2013), interacts directly with the mitochondrial membrane (Ping *et al.*, 2016). To test whether Mmr1 is also able to directly interact with phospholipid membranes, we examined the membrane-binding properties of Mmr1 in vitro. Recombinant Mmr1 was purified from *Escherichia coli*, and its ability to associate with liposomes that mimic the composition of the mitochondrial outer membrane was examined using liposome flotation assays. Specifically, we used individual phospholipids to make chemically defined liposomes that mimic the composition of the mitochondrial outer membrane (outer membrane composition; OMC) and varied the concentration of cardiolipin (CL) present in these liposomes (0%, 6%, and 17%). CL, a mitochondria-specific phospholipid, is reported to be present at 6% in the mitochondrial outer membrane and at 17% at contact sites between the mitochondrial outer and inner membranes (Simbeni *et al.*, 1991; Zinser and Daum, 1995). In flotation assays, recombinant Mmr1 associated with OMC liposomes containing 6 and 17% CL, but not with OMC liposomes that lack CL (Figure 1A).

To further examine the specificity of the Mmr1–phospholipid interaction, we assessed the ability of Mmr1 to bind liposomes composed of the neutral phospholipid phosphatidylcholine (PC) plus one of the following phospholipids: CL, phosphatidic acid (PA), phosphatidylglycerol (PG), phosphatidylinositol (PI), phosphatidylserine (PS), or phosphatidylethanolamine (PE). When individual phospholipids were present at 20 mol%, Mmr1 associated only with CL-containing liposomes (Figure 1B). When increased to 40 mol%, PA, PG, and PS were also able to support the Mmr1–phospholipid interaction. Increasing the salt concentration in the liposome flotation assays disrupted the Mmr1–phospholipid interaction, indicating that the interaction is electrostatic (Figure 1C). Together, these data indicate that Mmr1 can interact directly with phospholipid membranes in vitro and exhibits a preference for liposomes containing CL.

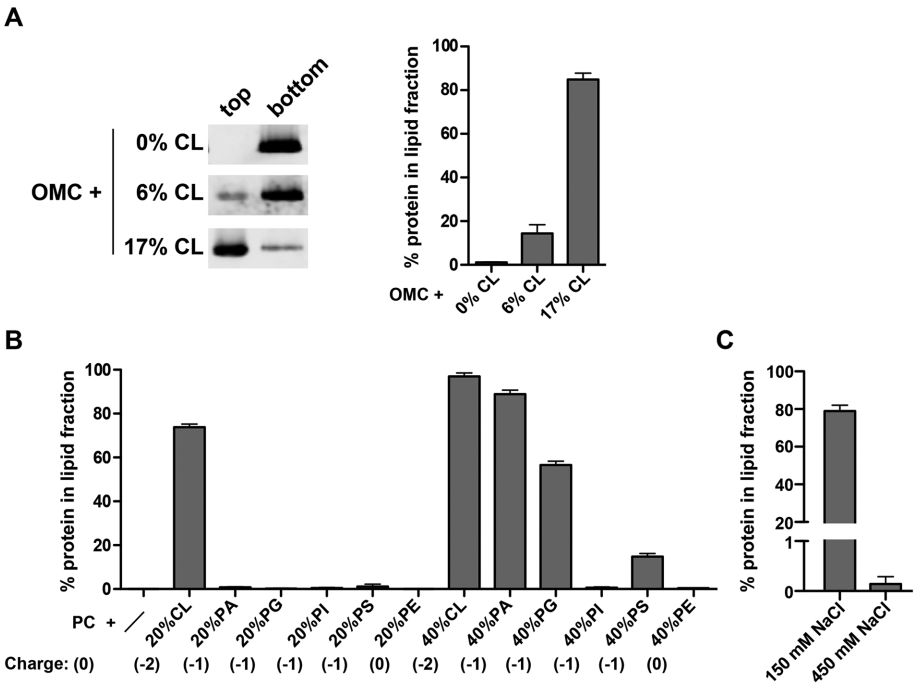

FIGURE 1: Mmr1 interacts directly with phospholipid membranes. (A) Purified Mmr1 (5 μM) was incubated with OMC liposomes containing 0, 6, and 17% CL, as indicated. The association of protein with liposomes was assessed by its ability to float with liposomes, as indicated by the amount of protein in the top fraction of the gradient. Equivalent amounts of the top and bottom fractions of the flotation gradients were subjected to SDS–PAGE and Western blot analysis (left panel). The percentage of protein found in the top fraction is shown as the mean ± SEM; $n = 3$ independent experiments. (B) Purified Mmr1 (5 μM) was incubated with liposomes composed of PC and the indicated mol% of a second phospholipid, and the reactions were subjected to liposome flotation and analyzed as described in A. Data are shown as the mean ± SEM; $n = 3$ independent experiments. The net charge of the phospholipid headgroups is indicated below the graph in parentheses. (C) Purified Mmr1 (5 μM) was incubated with PC + 20% CL liposomes in the presence of 150 or 450 mM NaCl. The reactions were subjected to liposome flotation and analyzed as described in A. Data are shown as the mean ± SEM; $n = 3$ independent experiments.

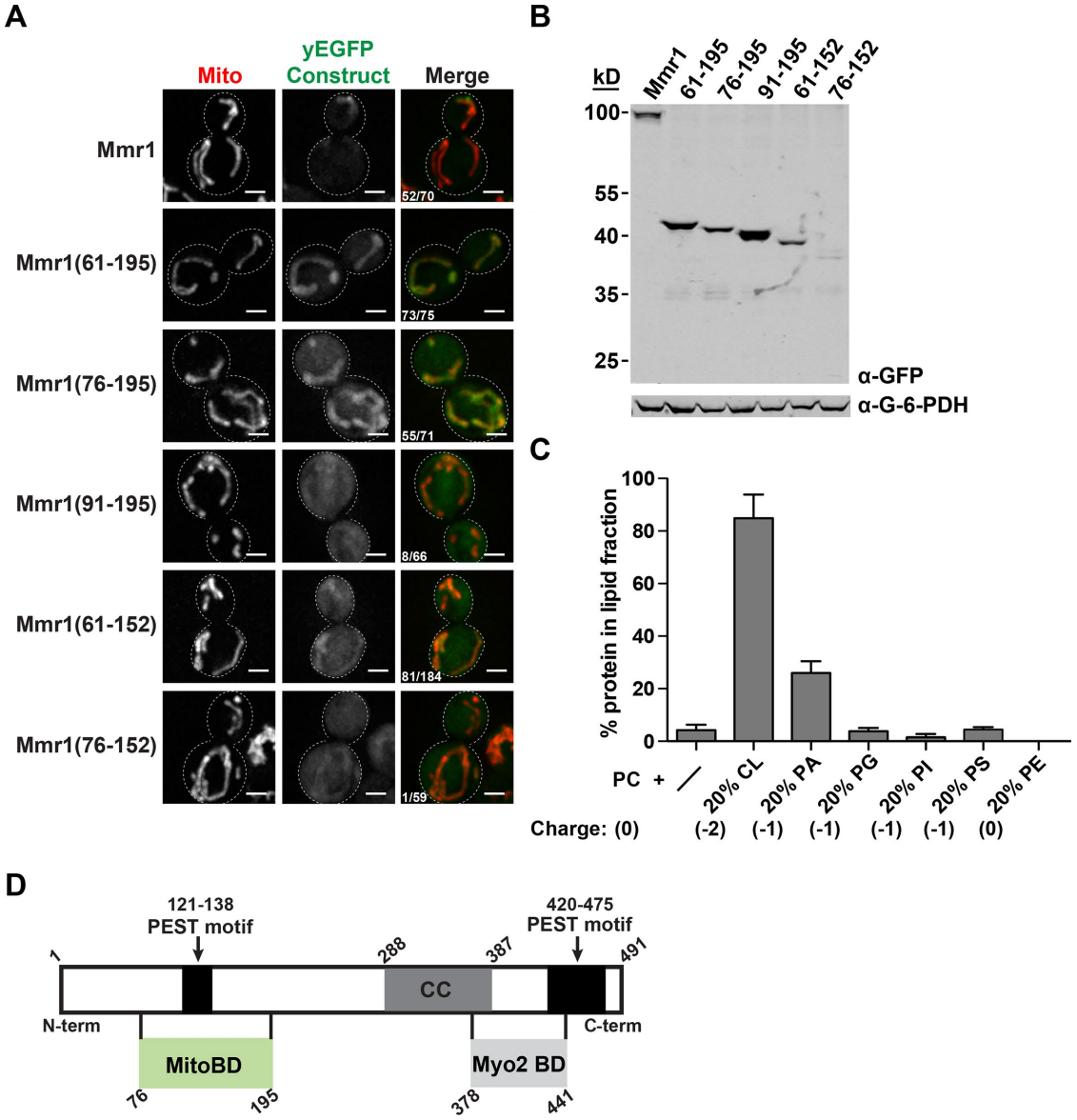

FIGURE 2: Amino acids 76–195 of Mmr1 are sufficient for the interaction with mitochondria. (A) Cells expressing mitoRED and the indicated Mmr1-yEGFP truncations were analyzed by fluorescence microscopy. Whole cell projections are shown. The cell cortex is outlined with a dashed white line. Scale bar, 2 μm. The number of cells in which the Mmr1-yEGFP truncation was observed to colocalize with mitochondria out of the total number of cells counted is shown in the bottom left corner of the merge image panel. (B) Whole cell extracts of strains expressing truncated forms of Mmr1-yEGFP, as indicated, were analyzed by SDS–PAGE and Western blot using anti-GFP to detect the Mmr1-yEGFP truncations and anti-G-6-PDH as a loading control. (C) Purified Mmr1(61–195)-GFP (5 μM) was incubated with liposomes composed of PC and the indicated mol% of a second phospholipid. The reactions were subjected to liposome flotation and analyzed as described in Figure 1A. Data are shown as the mean ± SEM; $n = 3$ independent experiments. The net charge of the phospholipid headgroups is indicated below the graph in parentheses. (D) Schematic of Mmr1. Myo2 BD, Myo2-binding domain; CC, coiled-coil; MitoBD, mitochondrial binding domain.

Mmr1(76–195) is necessary and sufficient for the interaction with mitochondria

Mmr1 lacks a predicted membrane-binding domain. To identify the membrane-binding domain within Mmr1, we expressed a series of Mmr1 truncations as yEGFP fusions from the endogenous *MMR1* locus and examined their localization relative to mitochondria (Figure 2A). Western blot analysis confirmed that the proteins were expressed with minimal degradation (Figure 2B). We based our truncations on the results of a previous study, which mapped the mitochondrial binding domain of Mmr1 to amino acids 61–355 (Itoh *et al.*, 2004), and on the results of structure prediction programs and regions of conservation. Consistent with previous studies, we observed that full-length Mmr1 colocalized with mitochondria and exhibited a punctate, bud-enriched localization (Figure 2A; Itoh *et al.*, 2004; Swayne *et al.*, 2011; Eves *et al.*, 2012). For the Mmr1 truncations, we found that Mmr1(61–195) colocalized with mitochondria, while the distribution of Mmr1(61–152) was shifted toward the cytosol. In addition, we found that Mmr1(76–195) colocalized with mitochondria but Mmr1(91–195) and Mmr1(76–152) were primarily cytosolic. In contrast to the polarized localization of wild-type Mmr1,

Mmr1(76–195) and the other mitochondrial-associated Mmr1 truncations appeared to be evenly distributed along mitochondria in the mother and bud (Figure 2A). These proteins lack the Myo2-binding domain, and their localization is consistent with the loss of Myo2-dependent bud-polarized localization (Itoh *et al.*, 2004; Eves *et al.*, 2012). Together, these results indicate that Mmr1(76–195) is sufficient for the interaction with mitochondria.

We next asked whether the minimal mitochondrial binding domain, Mmr1(76–195), was sufficient to interact with phospholipid membranes in vitro. Recombinant Mmr1(76–195) could not be stably expressed in *E. coli*. However, we were able to express and purify recombinant Mmr1(61–195) and test its ability to associate with phospholipid membranes using liposome flotation assays. Similar to full-length Mmr1, Mmr1(61–195) directly associated with liposomes and exhibited a preference for CL- and PA-containing phospholipid membranes (Figure 2C). Thus, our in vivo and in vitro studies indicate that amino acids 76–195 of Mmr1 compose the mitochondrial binding domain (mitoBD; Figure 2D).

We then examined whether our defined mitoBD was necessary for the Mmr1–mitochondria interaction in cells. We expressed Mmr1Δ76–195-yEGFP from the endogenous *MMR1* locus and examined the localization of the protein relative to mitochondria. We observed that Mmr1Δ76–195-yEGFP no longer colocalized with mitochondria (Figure 3A), consistent with the disruption of the Mmr1–mitochondria interaction. In addition, an enrichment of Mmr1Δ76–195-yEGFP in small buds was observed (Figure 3, A and B), indicating that deletion of the mitochondrial binding domain did not disrupt the overall folding of Mmr1 and the protein was still able to interact with Myo2. Western blot analysis confirmed that the protein was expressed with minimal degradation (Supplemental Figure S1A). As discussed below, Mmr1Δ76–195 was also able to interact with itself in yeast two-hybrid assays (Figure 4B), providing further evidence that deletion of amino acids 76–195 specifically disrupts the interaction between Mmr1 and mitochondria.

We next sought to identify amino acids within the mitoBD that when mutated disrupt the Mmr1–mitochondria interaction in vivo and examine how these mutations affect the ability of the protein to bind phospholipid membranes in vitro. Given the affinity of Mmr1 for negatively charged lipids, we identified basic amino acids within the Mmr1 mitoBD that are conserved and reversed the charge of these amino acids (Supplemental Figure S1B). Specifically, we constructed Mmr1 R80E R86E K95E K98E and will refer to this mutant as Mmr1^{4E}. When expressed as a yEGFP fusion in cells, Mmr1^{4E} no longer associated with mitochondria (Figure 3A and Supplemental Figure S1A), indicating the mutations interfere with the Mmr1–mitochondria interaction. In addition, the protein was found to be enriched in small buds, indicating that the interaction between Mmr1^{4E} and Myo2 was not disrupted (Figure 3, A and B). We then purified Mmr1^{4E} and tested its ability to interact directly with phospholipid membranes in vitro. In comparison to wild-type Mmr1, the association of Mmr1^{4E} with OMC+17% CL liposomes was dramatically reduced (Figure 3C). Thus, the inability of Mmr1^{4E} to associate with mitochondria in cells correlates with a defect in phospholipid membrane binding in vitro. Together, our data suggest that the Mmr1 mitoBD mediates a direct interaction between Mmr1 and the mitochondrial membrane.

Direct membrane binding contributes to Mmr1 function in mitochondrial inheritance

We next assessed mitochondrial inheritance in cells expressing Mmr1Δ76–195-yEGFP and Mmr1^{4E}-yEGFP. In the absence of Mmr1, a greater fraction of small-budded cells are devoid of mitochondria in comparison to wild-type cells, indicative of a delay in the inheritance of mitochondria (Itoh *et al.*, 2004). We found that cells expressing Mmr1Δ76–195-yEGFP and Mmr1^{4E}-yEGFP exhibit a delay in mitochondrial inheritance similar to that observed for cells lacking Mmr1 (Figure 3D). In the absence of Mmr1, Myo2-driven mitochondrial inheritance is dependent on the Myo2 adaptor protein Ypt11, and in the absence of both Ypt11 and Mmr1, cells are inviable or severely impaired for growth (Itoh *et al.*, 2004; Frederick *et al.*, 2008; Chernyakov *et al.*, 2013). Consistent with direct membrane binding of Mmr1 being critical for its function in mitochondrial inheritance, *mmr1Δ76–195Δypt11* and *mmr1*^{4E}*Δypt11* cells exhibited growth defects similar in severity to Δ*mmr1Δypt11* cells (Figure 3E). Together, these data indicate a direct interaction between Mmr1 and the mitochondrial membrane is critical for Mmr1 function in mitochondrial inheritance.

The coiled-coil domain of Mmr1 is necessary and sufficient for Mmr1 self-interaction

Our structure–function analysis of Mmr1 identified an unpredicted membrane-binding region within the protein, adding another functional domain to Mmr1 in addition to a well-characterized Myo2-binding domain and two putative PEST motifs (Figure 2D; Itoh *et al.*, 2004; Eves *et al.*, 2012). Mmr1 also contains a predicted coiled-coil (CC) domain (Itoh *et al.*, 2004). Although the CC domain of Mmr1 is suggested to be important for the function of the protein (Itoh *et al.*, 2004), it is not clear how the CC domain contributes to Mmr1 function. Intermolecular self-interaction has been suggested to be necessary for the function of the mitochondrial tethering protein Num1 and the Myo2 adaptor protein Smy1, and likely serves to increase the avidity of the proteins for their binding partners. For both Num1 and Smy1, the CC domains of the proteins mediate self-interaction (Tang *et al.*, 2012; Lwin *et al.*, 2016; Ping *et al.*, 2016). To determine whether the CC domain of Mmr1 mediates self-interaction, we examined the ability of Mmr1 to self-interact using a yeast two-hybrid assay conducted in Δ*mmr1* cells. Thus, the activation and binding domain fusions of Mmr1 were the only source of Mmr1 protein in the cells. We were able to detect an Mmr1–Mmr1 interaction in this assay (Figure 4A). Using a series of truncated Mmr1 constructs, we determined that the CC domain of Mmr1, amino acids 288–387, was sufficient for self-interaction (Figure 4A). Because the CC domain partially overlaps with the Myo2-binding domain, we wanted to create an Mmr1 construct that was able to interact with Myo2 but not with itself to test the functional significance of self-interaction. Therefore, we constructed Mmr1Δ288–377 (referred to as Mmr1ΔCC), in which the vast majority of the CC domain is deleted but the Myo2-binding domain is left intact (Eves *et al.*, 2012). Indeed, this construct was able to interact with Myo2 but not itself, full-length Mmr1, or Mmr1Δ76–195 (Figure 4, B and C). These results suggest that the CC domain is necessary and sufficient for Mmr1 self-interaction but is not required for the interaction with Myo2.

To further test the idea that the CC domain mediates Mmr1 self-interaction, we examined the ability of Mmr1ΔCC to self-interact in cells using coimmunoprecipitation assays. We coexpressed differentially tagged versions of Mmr1ΔCC in diploid cells and examined the ability of Mmr1ΔCC-FLAG to coimmunoprecipitate Mmr1ΔCC-yEGFP. In comparison to the steady-state levels of wild-type Mmr1-FLAG and Mmr1-yEGFP, the steady-state levels of Mmr1ΔCC-FLAG and Mmr1ΔCC-yEGFP expressed from the endogenous *MMR1* promoter were increased (Figure 4D; lysate). Despite the increased levels of the Mmr1ΔCC proteins, the ability of Mmr1ΔCC-FLAG to coimmunoprecipitate Mmr1ΔCC-yEGFP was dramatically reduced compared with the ability of Mmr1-FLAG to coimmunoprecipitate Mmr1-yEGFP (Figure 4, D and E). These results further support the idea that the CC domain of Mmr1 mediates Mmr1 self-interaction.

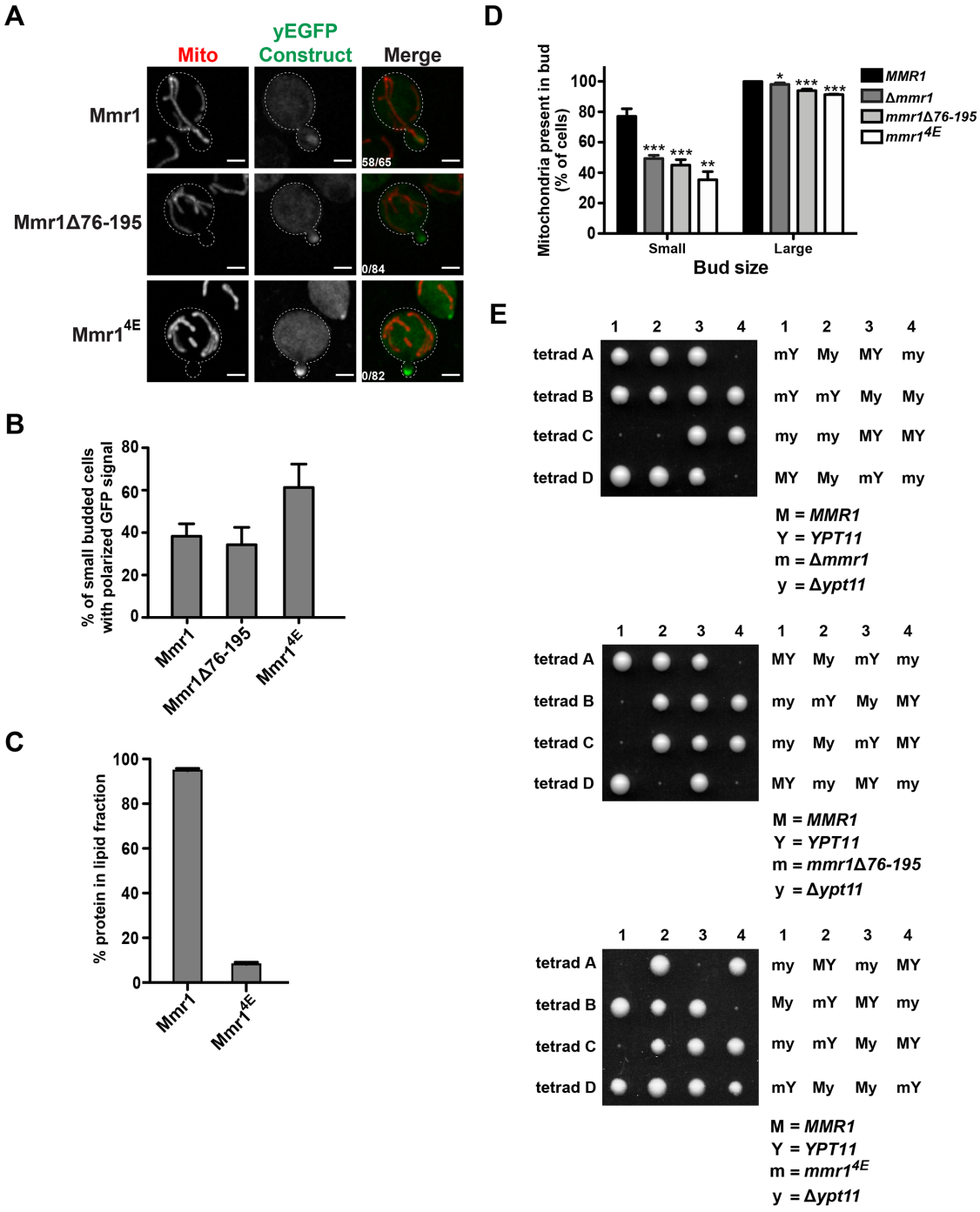

FIGURE 3: The membrane-binding domain of Mmr1 is required for Mmr1 function. (A, B) Cells expressing mitoRED and Mmr1-yEGFP, Mmr1Δ76–195-yEGFP, or Mmr1^{4E}-yEGFP were analyzed by fluorescence microscopy. Whole cell projections are shown in A. The cell cortex is outlined with a dashed white line. Scale bar, 2 μm. The number of cells in which the yEGFP fusion was observed to colocalize with mitochondria out of the total number of cells counted is shown in the bottom left corner of the merge image panel. Quantification of the polarized localization of the yEGFP fusion proteins in small-budded cells is shown as the mean ± SD in B; $n = 3$ independent experiments in which ≥78 small-budded cells were counted. (C) Purified Mmr1 and Mmr1^{4E} (5 μM) were incubated with OMC + 17% CL liposomes. The reactions were subjected to liposome flotation and analyzed as described in Figure 1A. Data are shown as the mean ± SEM; $n = 3$ independent experiments. (D) The presence of mitochondria in small and large buds was quantified in cells expressing wild-type Mmr1-yEGFP, Mmr1Δ76–195-yEGFP, and Mmr1^{4E}-yEGFP along with mitoRED. Buds were classified based on the bud-to-mother-diameter ratio: small buds have a bud/mother-diameter ratio of <1/3 and large buds have a bud/mother-diameter ratio of ≥1/3. Data are shown as the mean ± SD; $n = 3$ independent experiments in which ≥84 cells were counted for each bud size. p values are in comparison to *MMR1* cells of the comparable bud size. ***, $p < 0.001$; **, $p < 0.01$; *, $p < 0.05$. (E) Δ*ypt11*Δ*mmr1*, Δ*ypt11 mmr1*Δ*76–195-yEGFP*, and Δ*ypt11 mmr1*^{4E}*-yEGFP* diploid cells were sporulated, and spores from individual tetrads were arranged in a row on YPD medium. Growth on selective plates was used to score the markers for the deletions and yEGFP fusion and determine the genotypes of the haploid cells, which are indicated.

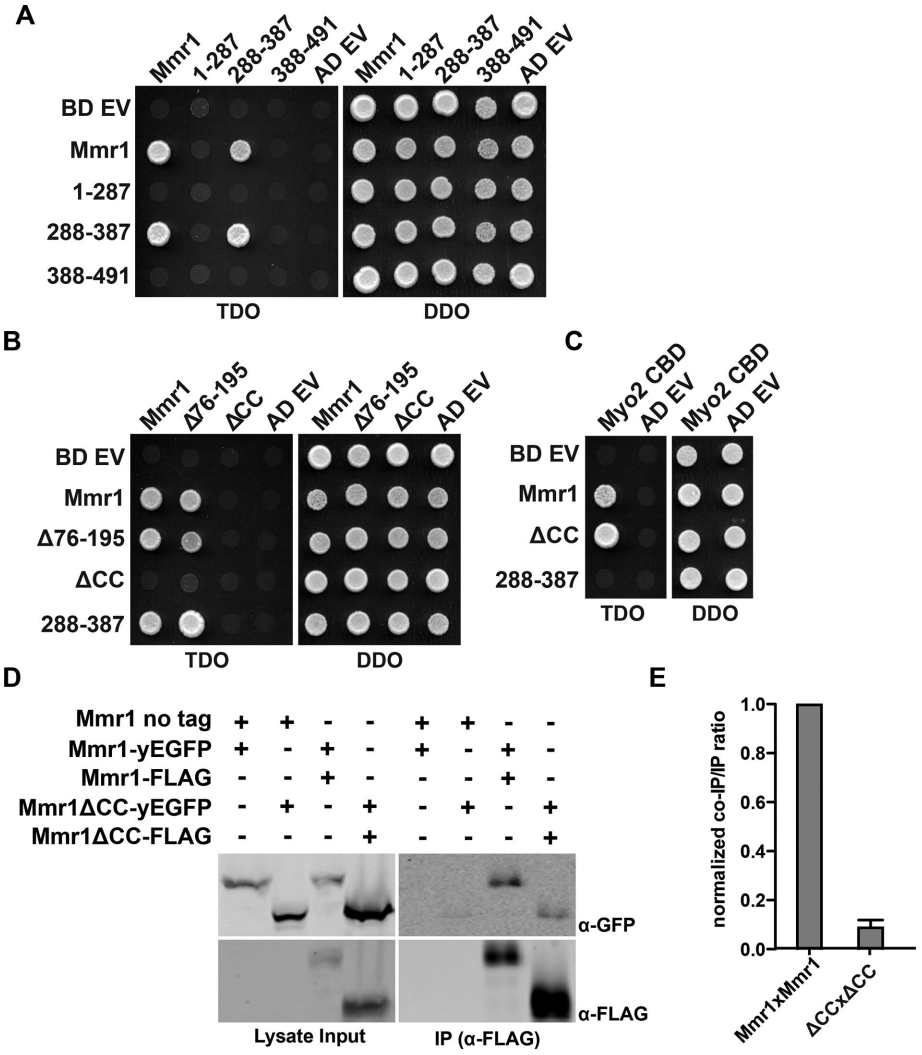

FIGURE 4: Mmr1 self-interaction is mediated by the CC domain. (A–C) Yeast two-hybrid assays to assess interactions between the indicated regions of Mmr1 (A), the ability of Mmr1Δ76–195 and Mmr1ΔCC to self-interact (B), and interactions between Mmr1ΔCC and the Myo2 cargo-binding domain (CBD) (C). For all yeast two-hybrid assays, protein–protein interactions were assessed by growth on triple-dropout (TDO) medium. AD EV, activation domain empty vector; BD EV, binding domain empty vector; TDO, SC–Leu–Trp–Ade; double-dropout medium (DDO), SC–Leu–Trp. (D, E) Cell lysates from diploid cells expressing Mmr1-FLAG and Mmr1-yEGFP or Mmr1ΔCC-FLAG and Mmr1ΔCC-yEGFP were subjected to anti-FLAG immunoprecipitation (IP). Cell lysates and IP elutions were analyzed by SDS–PAGE and Western blot using anti-FLAG and anti-GFP antibodies (D). Quantification of the normalized co-IP/IP ratio is shown in E as the mean ± SD, $n = 3$ independent experiments.

Self-interaction contributes to Mmr1 function in mitochondrial inheritance

To test the functional significance of Mmr1 self-interaction, we examined the localization of Mmr1ΔCC-yEGFP and mitochondrial inheritance in these cells. In comparison to the punctate, bud-enriched localization of Mmr1-yEGFP, Mmr1ΔCC-yEGFP localized more evenly along mitochondria in both the mother and bud with less bud enrichment (Figure 5A). Thus, the CC domain is required for the proper distribution of Mmr1 within cells but is not required for the association with mitochondria. Cells expressing Mmr1ΔCC also exhibited subtle, nonsignificant defects in mitochondrial inheritance in otherwise wild-type and Δ*ypt11* backgrounds (Figure 5B), suggesting the function of Mmr1ΔCC in mitochondrial inheritance may be attenuated.

On the basis of our coimmunoprecipitation experiments, we noted that the levels of Mmr1ΔCC-yEGFP were higher than those of wild-type Mmr1-yEGFP. Indeed, the steady-state protein levels of Mmr1ΔCC-yEGFP were found to be ~16× that of Mmr1-yEGFP (Supplemental Figure S2, A and C). These results are consistent with the previous finding that disrupting the polarized localization of Mmr1 results in higher steady-state levels of the protein (Eves *et al.*, 2012). In addition, these results raise the possibility that overexpression of the protein may be compensating for its attenuated function, decreasing the severity of the phenotypes observed. Therefore, we sought to examine the function of Mmr1ΔCC-yEGFP when expressed at levels more similar to wild-type Mmr1. To this end, we placed a GalS promoter upstream of *MMR1-yEGFP* and *MMR1ΔCC-yEGFP* and engineered the strains to express a transcription factor that drives expression from the Gal promoter only in the presence of estradiol. The concentrations of estradiol were optimized so that the steady-state levels of Mmr1-yEGFP and Mmr1ΔCC-yEGFP were comparable to that of Mmr1-yEGFP expressed from the endogenous *MMR1* promoter (Figure 5C and Supplemental Figure S2, B and C). Cells expressing Mmr1-yEGFP from the estradiol-regulated GalS promoter inherited mitochondria similarly to cells expressing Mmr1-yEGFP from the endogenous Mmr1 promoter (Figure 5, B and D). In contrast, cells expressing Mmr1ΔCC-yEGFP from the estradiol-regulated GalS promoter exhibited a defect in mitochondrial inheritance similar in severity to that observed in Δ*mmr1* cells (Figures 3D and 5D). These results indicate that, at wild-type levels of Mmr1, the CC domain is critical for Mmr1-mediated mitochondrial inheritance, and the function of the CC domain can be bypassed by overexpression of the protein.

Interestingly, we found that the CC domain was also necessary for the polarized localization of the Mmr1 Myo2 BD. Specifically, we expressed Mmr1(288–491), which contains both the CC domain and Myo2 BD, and Mmr1(378–491), which contains only the Myo2 BD, as yEGFP fusions (Supplemental Figure S2D). In contrast to the striking bud-polarized localization of Mmr1(288–491)-yEGFP, Mmr1(378–491)-yEGFP was evenly distributed in the cytosol of the mother and bud (Figure 5, E and F), consistent with previous findings (Itoh *et al.*, 2004). To test whether CC-mediated dimerization specifically was necessary for the polarized localization of the Mmr1 Myo2 BD, we replaced amino acids 288–377 of Mmr1 with the CC domain of GCN4, which forms a well-characterized homodimer (O'Shea *et al.*, 1991). Notably, the addition of the GCN4CC to Mmr1(378–491)-yEGFP partially restored the bud-polarized localization of the protein (Figure 5, E and F). In contrast to the localization of Mmr1(288–491)-yEGFP, which robustly accumulated at the bud tip of small-budded cells, GCN4CC-Mmr1(378–491)-yEGFP

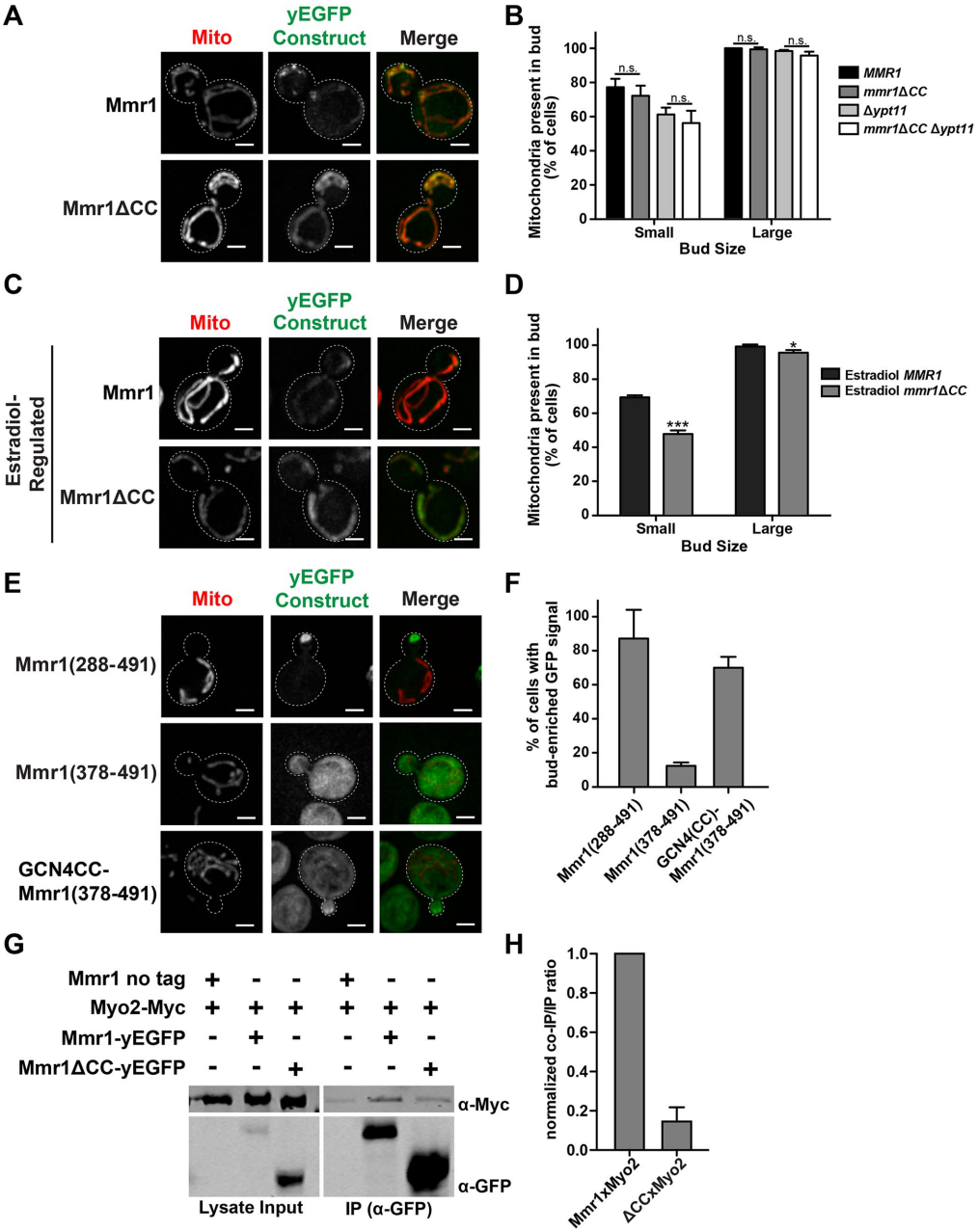

FIGURE 5: The CC domain of Mmr1 is required for Mmr1 function. (A, B) Cells expressing mitoRED and Mmr1-yEGFP and Mmr1ΔCC-yEGFP, as indicated, were analyzed by fluorescence microscopy (A), and the presence of mitochondria in small and large buds was quantified as described in Figure 3D (B). Whole cell projections are shown. The cell cortex is outlined with a dashed white line. Scale bar, 2 μm. Data are shown as the mean ± SD; $n = 3$ independent experiments in which ≥86 cells were counted for each bud size. n.s., not significant. (C, D) Cells expressing mitoRED and Mmr1-yEGFP or Mmr1ΔCC-yEGFP from an estradiol-regulated GalS promoter were grown in the presence of 0.5 and 0.05 nM estradiol, respectively. The cells were analyzed by fluorescence microscopy (C), and the presence of mitochondria in small and large buds was quantified as described in Figure 3D (D). Whole cell projections are shown. The cell cortex is outlined with a dashed white line. Scale bar, 2 μm. Data are shown as the mean ± SD; $n = 3$ independent experiments in which ≥86 cells were counted for each bud size. p values are in comparison to estradiol *MMR1* cells of the comparable bud size. ***, $p < 0.001$; *, $p < 0.05$. (E, F) Cells expressing mitoRED and Mmr1(288–491)-yEGFP, Mmr1(378–491)-yEGFP, or GCN4CC-Mmr1(378–491), as indicated, were analyzed by fluorescence microscopy. Whole cell projections are shown in E. The cell cortex is outlined with a dashed white line. Scale bar, 2 μm. Quantification of small-budded cells with a bud-enriched localization of the yEGFP fusion protein is shown as the mean ± SD in F; $n = 3$ independent experiments in which ≥79 small-budded cells were counted. Any cell with an enrichment of the protein at the bud tip above the cytosolic signal was counted as bud-enriched. (G, H) Cell lysates from cells expressing Myo2-Myc and either Mmr1-yEGFP or Mmr1ΔCC-yEGFP were subjected to anti-GFP immunoprecipitation (IP). Cell lysates and IP elutions were analyzed by SDS–PAGE and Western blot using anti-GFP and anti-Myc antibodies. Quantification of the normalized co-IP/IP ratio is shown in H as the mean ± SD, $n = 3$ independent experiments.

localized diffusely in the cytosol as well as in accumulations at the bud tip. The percentage cells with an enrichment of the protein at the bud tip was similar for both Mmr1(288–491)-yEGFP and GCN4CC-Mmr1(378–491)-yEGFP (Figure 5F). These results suggest that, even though constructs lacking the CC domain can interact with Myo2 (Figure 4C; Eves *et al.*, 2012), dimerization driven by the CC domain plays a role in the Myo2-dependent polarization of the protein.

To further test the idea that CC-mediated dimerization of Mmr1 enhances the interaction with Myo2, we examined the interaction between Mmr1ΔCC and Myo2 in cells using coimmunoprecipitation assays. We found that despite the increased levels of Mmr1ΔCC in cells, the ability of Mmr1ΔCC to coimmunoprecipitate Myo2 was reduced compared with the ability of Mmr1 to coimmunoprecipitate Myo2 (Figure 5, G and H). Together, our results suggest that self-interaction mediated by the CC domain is necessary for Mmr1 function in mitochondrial inheritance and likely functions to enhance the interaction between Mmr1 and Myo2.

DISCUSSION

Here we provide evidence demonstrating that direct membrane binding and self-interaction are critical for Mmr1 function in mitochondrial inheritance. Interestingly, these functional features are shared between Mmr1 and Num1, the core protein component of MECA. Both proteins exhibit the ability to directly interact with phospholipid membranes via unpredicted lipid-binding domains and the ability to self-assemble (Tang *et al.*, 2012; Ping *et al.*, 2016). As proposed for Num1 (Kraft and Lackner, 2017), self-assembly of Mmr1 likely increases the avidity between Mmr1 and its binding partners. Indeed, our data suggest that Mmr1 self-interaction facilitates a robust interaction between Mmr1 and Myo2. The finding that overexpression of Mmr1ΔCC bypasses the function of the CC domain is consistent with the idea that the CC domain and Mmr1 self-interaction are not required for the interaction with Myo2 but enhance the interaction. Self-interaction likely also enhances the interaction between Mmr1 and mitochondria by increasing the number of membrane-binding sites per functional unit and, therefore, the avidity of Mmr1 for the membrane. In contrast to a previous study that includes the CC domain as part of the mitochondrial and Myo2-binding domains (Itoh *et al.*, 2004), our data indicate that the CC domain is not required for Mmr1–mitochondria and Mmr1–Myo2 interactions but instead likely impacts the robustness of these interactions. Two conserved residues in the mitochondrial binding domain and one conserved residue in the CC domain of Mmr1 have been identified as sites of phosphorylation (Swaney *et al.*, 2013). We predict the spatial and temporal regulation of phosphorylation at these sites will serve as a mechanism to regulate Mmr1-binding partner interactions and, consequently, Mmr1 function in space and time.

Similar to Num1 (Ping *et al.*, 2016), in vitro Mmr1 and the Mmr1 mitoBD preferentially bind phospholipid membranes enriched in CL and also show preferential binding to PA. Like CL, PA is a negatively charged, cone-shaped lipid. Cone-shaped, or nonbilayer lipids, induce membrane curvature or create distinct microenvironments in a planar bilayer (van den Brink-van der Laan *et al.*, 2004; Osman *et al.*, 2011). Therefore, we speculate that Mmr1, rather than recognizing a specific phospholipid, recognizes a membrane structure that is formed or reinforced by CL, PA, and likely other lipid and protein factors. Consistent with this idea, noticeable defects in the association of Mmr1 or the Mmr1 mitoBD with mitochondria are not observed in cells that lack CL (Supplemental Figure S3, A and B). In addition, genetic interactions between *ypt11* and CL synthesis mutants are not observed (Supplemental Figure S3C). Additional factors have been proposed to compensate for the lack of CL when CL synthesis is disrupted. For example, PE, a cone-shaped but neutral lipid, as well as PG, a CL precursor, have overlapping functions with and can substitute for CL (Chang *et al.*, 1998; Gohil *et al.*, 2005; Joshi *et al.*, 2012). In cells lacking Ups1, a protein that functions early in the CL synthesis pathway, CL levels decrease and PA levels increase, most notably at contact sites between the outer and inner membranes (Connerth *et al.*, 2012). The idea that other factors can compensate for CL is further supported by the finding that Mgm1, a protein that drives the fusion of mitochondria, preferentially binds to CL in vitro and its activity is stimulated by CL in vitro, but CL is not essential for mitochondrial fusion in cells (DeVay *et al.*, 2009; Chen *et al.*, 2010; Joshi *et al.*, 2012). Thus, multiple lines of evidence suggest additional factors can compensate for the lack of CL in cells. Although our data indicate that Mmr1 can directly bind phospholipid membranes and that direct membrane binding contributes to Mmr1 function, we cannot exclude the possibility that mitochondrial proteins may contribute to the Mmr1–mitochondria interaction.

Interestingly, the relationship between Mmr1 and Num1 function in mitochondrial positioning changes over the course of the cell cycle. Our previous work demonstrates that mitochondria drive the assembly of Num1 clusters. In the absence of mitochondrial inheritance, Num1 clusters do not form in buds. The lack of Num1 clusters not only disrupts mitochondria–plasma membrane anchoring in large buds but also Num1-mediated dynein anchoring and, consequently, dynein-mediated spindle positioning (Kraft and Lackner, 2017). Therefore, what starts out as an antagonistic relationship between Mmr1 function in the bud and Num1 function in the mother early in the cell cycle turns into a facilitatory relationship in which the anchoring functions of Num1 in large buds are positively impacted by Mmr1-mediated mitochondrial inheritance later in the cell cycle. Therefore, the spatial and temporal regulation of Mmr1 function not only impacts mitochondrial positioning but also the formation of a mitochondria–plasma membrane anchor that functions in dynein-mediated nuclear positioning. In this context, we speculate that the functional connections and dependencies between two mitochondrial positioning pathways and a nuclear positioning pathway provide a means to order and integrate major spatial organization pathways within the cell.

MATERIALS AND METHODS

Strains and plasmids

Strain W303 (*ade2–1*; *leu2–3*; *his3–11*, *15*; *trp1–1*; *ura3–1*; *can1–100*; Naylor *et al.*, 2006) and the yeast two-hybrid strains PJ69-4A and PJ69-4alpha (MATa/alpha *trp1-901 leu2-3,112 ura3-52 his3-200Δgal4Δgal80 LYS2::GAL1-HIS3 GAL2-ADE2 met2::GAL7-lacZ* (gifts from S. Fields, University of Washington, and the Yeast Resource Center; James *et al.*, 1996) were described previously. Tables of the strains, plasmids, and primers used in this study can be found in the Supplemental Material.

The following W303, PJ69-4A, and PJ69-4alpha gene deletion strains were obtained by replacing the complete ORF of the genes with the indicated cassette using PCR-based targeted homologous recombination: W303 Δ*ypt11::NATNT2*, W303 Δ*mmr1::KANMX6*, W303 Δ*crd1::KANMX6*, W303 Δ*cld1::KANMX6*, W303 Δ*taz1::NATNT2*, PJ69-4A Δ*mmr1::NATNT2*, and PJ69-4alpha Δ*mmr1::NATNT2* (Longtine *et al.*, 1998; Janke *et al.*, 2004). The functional C-terminally tagged strains *MMR1-yEGFP::HIS* (Mmr1-yEGFP), *MMR1-FLAG::HIS* (MMR1-FLAG), and *Myo2-Myc::HIS* were constructed by PCR-based targeted homologous recombination using pFA6a-link-*yEGFP::SpHIS5* (pKT128), pFA6a-FLAG-His3MX6, and pFA6a-13Myc-His3MX6 (Sheff and Thorn, 2004; Hoppins *et al.*, 2011).

MMR1(61-195)-yEGFP::HIS, MMR1(76–195)-yEGFP::HIS, *MMR1(91–195)-yEGFP::HIS*, *MMR1(61–152)-yEGFP::HIS*, *MMR1(76–152)-yEGFP::HIS*, *MMR1(288–491)-yEGFP::HIS*, *MMR1(378–491)-yEGFP::HIS*, and *GCN4CC-Mmr1(378–491)-yEGFP::HIS* were constructed by PCR-based targeted homologous recombination in which two PCR products were transformed into Δ*mmr1::KANMX6*. PCR product #1 encoded the indicated *MMR1* coding region with homology to the genome upstream of the *MMR1* locus at the 5′ end and homology to the yEGFP cassette at the 3′ end. PCR product #2 encoded the *yEGFP::SpHIS5* cassette with homology to the end of the *MMR1* truncation at the 5′ end and homology to the genome downstream from the *MMR1* locus at the 3′ end. For *GCN4CC-Mmr1(378–491)-yEGFP::HIS*, a gBlock containing the *GCN4CC-Mmr1(378–491)* sequence was used as the template for PCR product #1. The GCN4 CC sequences encodes amino acids 249–281 of GCN4 and is fused to Mmr1(378–491) via a GA linker (O'Shea *et al.*, 1991).

MMR1(Δ76–195)-yEGFP::HIS, *MMR1(Δ288–377)-yEGFP::HIS* (referred to as Mmr1ΔCC-yEGFP), *MMR1(Δ288–377)-FLAG::HIS* (referred to as Mmr1ΔCC-FLAG), and *MMR1*4E-*yEGFP::HIS* were constructed by PCR-based targeted homologous recombination in which three PCR products were transformed into Δ*mmr1::KANMX6*. PCR product #1 encoded the *MMR1* coding sequence upstream of the deletion with homology to the genome upstream of the *MMR1* locus at the 5′ end and homology to PCR product #2 at the 3′ end. PCR product #2 encoded the *MMR1* coding sequence downstream from the deletion with homology to PCR product #1 at the 5′ end and homology to PCR product #3 at the 3′ end. PCR product #3 encoded the *yEGFP::SpHIS5* or *FLAG::SpHIS5* cassette with homology to the end of the *MMR1* truncation at the 5′ end and homology to the genome downstream from the *MMR1* locus at the 3′ end. For *MMR1*4E-*yEGFP::HIS*, a gBlock containing the sequence encoding amino acids 1–195 of Mmr1 with the R80E R86E K95E K98E mutations was used as the template for PCR product #1.

To regulate *MMR1-yEGFP* and *MMR1ΔCC-yEGFP* expression using estradiol, the GalS promotor was placed upstream of the *MMR1* coding sequence in the genome. The GalS::*MMR1-yEGFP*::NAT::HIS and GalS::*MMR1ΔCC-yEGFP*::NAT::HIS strains were constructed by PCR-based targeted homologous recombination using pYM-N31 (Janke *et al.*, 2004) and the *MMR1-yEGFP::HIS* and *MMR1ΔCC-yEGFP::HIS* strains described above. The strains were then transformed with Mss1-linearized pAGL. pAGL encodes for GAL4-EstrogenBD-VP16::NATMX6, which is the transcription factor used for estradiol control of GAL promoters (Veatch *et al.*, 2009).

Haploid double-mutant/tagged strains were generated by mating, followed by sporulation and tetrad analysis or by PCR-based targeted homologous recombination.

The plasmids pXY142-mitodsRED (mitoRED; Friedman *et al.*, 2011), pAGL (Veatch *et al.*, 2009), pET22b His6-T7 (Ping *et al.*, 2016), pWaldo-GFPd (a gift from Heather Pinkett, Northwestern University; Drew *et al.*, 2006), pGADC1-Myo2 cargo-binding domain (CBD; Pashkova *et al.*, 2005), and pGBKT7-BamHI and pGADT7-BamHI (Lackner *et al.*, 2013) were described previously.

pET22b His6-T7 and pWaldo-GFPd modMCS were used to overexpress proteins in *E. coli*. To construct pET22b His6-T7-Mmr1 and pET22b His6-T7-Mmr1^{4E}, Mmr1 and Mmr1^{4E} were PCR amplified from genomic DNA isolated from W303 and W303 *MMR1*4E-*yEGFP*, digested with *Bgl*II and *Xho*I, and cloned into pET22b His6-T7, which was digested with *Bam*HI and *Xho*I. To construct pWaldo Mmr1(61–195)-GFP, pWaldo-GFPd modMCS was first constructed by modifying the multiple cloning site to 5′-CATATGGGATCCACTAGTGTCGACCTCGAGAGATCC-3′ using annealed oligos. The annealed oligos containing *Nde*I and *Bgl*II overhangs were inserted into pWaldo-GFPd that had been digested with *NdeI* and *Bam*HI. This resulted in the destruction of the original *Bam*HI site in the vector. Mmr1(61–195) was PCR amplified from pGADT7 Mmr1 and cloned into pWaldo-GFPd modMCS using *Bam*HI and *Xho*I sites.

pGADT7-BamHI Mmr1, Mmr1Δ76–195, and Mmr1ΔCC and pGBKT7-BamHI Mmr1Δ76-195 and Mmr1ΔCC were constructed by inserting the indicated Mmr1 coding sequence into pGADT7-BamHI or pGBKT7-BamHI by GAP repair. All other pGADT7-BamHI and pGBKT7-BamHI Mmr1 constructs were constructed by amplifying the indicated Mmr1 coding sequence by PCR and inserting the *Bgl*II/*Xho*I digested product into pGADT7-BamHI and pGBKT7-BamHI using *Bam*HI/*Xho*I and *Bam*HI/*Sal*I, respectively.

Imaging

For Figures 2, 3, and 5, the indicated cells harboring mitoRED were grown to mid–log phase in SC-LEU + 2% (wt/vol) dextrose media with 2× adenine. For Figure 5D, 0.5 nM estradiol and 0.05 nM estradiol were added to the GalS::Mmr1-yEGFP and GalS::Mmr1ΔCC-yEGFP cultures, respectively, 5 h before imaging.

For all imaging, cells were grown as described above at 24°C, concentrated by centrifugation, and mounted on a 4% wt/vol agarose pad. All imaging was performed at 22°C. Z series of cells were imaged at a single time point using a spinning disk confocal system (Leica) fit with a spinning disk head (CSU-X1; Yokogawa), a PLAN APO 100× 1.44 NA objective (Leica), and an electron-multiplying charge-coupled device camera (Evolve 512 Delta; Photometrics). A step size of 0.4 µm was used. Image capture was done using Metamorph (Molecular Devices). The images were deconvolved using AutoQuant X3's (Media Cybernetics) iterative, constrained 3D deconvolution method. Fiji (National Institutes of Health) and Photoshop (Adobe) were used to make linear adjustments to brightness and contrast. Deconvolved images are shown.

For the quantification of mitochondrial inheritance and the polarized localization of yEGFP fusion proteins in small buds, buds were classified as follows: small buds have a bud/mother-diameter ratio of <1:3, and large buds have a bud/mother-diameter ratio of ≥1:3. For mitochondria to be scored as properly inherited, mitochondria need to cross the mother–bud neck. Measurements of bud size were done using Fiji.

Protein purification

Mmr1, Mmr1^{4E}, and Mmr1(61–195) were purified from *E. coli* as follows. Starter cultures of BL21(λDE3)/RIPL cells harboring plasmids pET22b His6-T7-Mmr1, pET22b His6-T7-Mmr1^{4E}, or pWaldo Mmr1(61–195)-GFP-His8, from which the expression of the genes is driven by the T7 promoter**,** were grown overnight in Luria-Bertani (LB) medium with chloramphenicol (25 µg/ml), glucose (0.04%), and ampicillin (150 µg/ml) for pET22b or kanamycin (50 µg/ml) for the Waldo vector. The starter cultures were used to inoculate 2 l of LB medium containing the same additions described above. The cells were grown at 37°C until an OD_{600} of 0.5 was reached. To induce protein expression, isopropyl β-D-1-thiogalactopyranoside (IPTG) was added to a final concentration of 250 µM, and the cultures were grown for 2 h at 30°C for His6-T7-Mmr1 and His6-T7-Mmr1^{4E} and 16 h at 18°C for Mmr1(61–195)-GFP-His8. The cells were then harvested by velocity centrifugation at 5000 × *g* for 15 min. The resulting pellet was resuspended in 1/200 volume of resuspension buffer (RB; 20 mM HEPES, pH 7.0, 500 mM NaCl, 1.89 mM BME) +1X Protease Inhibitor Cocktail Set 1 (PIC; Millipore), quickly frozen in liquid N_2, and stored at −80°C. The cell suspension was quickly

thawed in a room temperature water bath, PIC was added to 1X, and the thawed cell suspension was subjected to two more freeze-thaw cycles. The homogenate was sonicated briefly to further lyse cells and clarified by centrifugation at 17,000 × *g* for 45 min at 4°C. The proteins were purified from the supernatant using HisPur Ni-NTA resin (Thermo Scientific). The supernatant was incubated with resin for 1 h at 4°C, and the resin was then pelleted at 3000 × *g* for 3 min. The protein bound resin was washed three times with RB+1X PIC and three times with wash buffer (RB + 30 mM imidazole + 0.25X PIC) and was then loaded into a chromatography column. Protein was eluted from the column using a step gradient of RB + 60–300 mM imidazole. Each elution (5 µl) was mixed with sample buffer, run on a SDS–PAGE gel, and Coomassie stained. Mmr1, Mmr1^{4E}, or Mmr1(61–195) elutions were pooled and dialyzed overnight in 20 mM HEPES, pH 7.0, 500 mM NaCl. Glycerol was added to 10%, and the protein was aliquoted, frozen in liquid N_2, and stored at −80°C. The concentration of the purified proteins was determined using a bicinchoninic acid (BCA) protein assay kit (Pierce).

Liposome flotation assays

The following phospholipids were supplied in chloroform at 10 mg/ml from Avanti Polar Lipids: 1-palmitoyl-2-oleoyl-sn-glycero-3-phosphate (PA), palmitoyl-oleoyl phosphatidylcholine (PC), palmitoyl-oleoyl phosphatidylethanolamine (PE), 1,2-dioleoyl-*sn*-glycero-3-phospho-(1′-*rac*-glycerol) (PG), soybean phosphatidylinositol (PI), 1-palmitoyl-2-oleoyl-sn-glycero-3-(phosphor-L-serine) (PS), and tetraoleoyl-cardiolipin (CL). For OMC liposomes, individual phospholipids were mixed to achieve a mol% composition that mimics the mitochondrial outer membrane: 46% PC, 33% PE, 10% PI, 4% PA, 1% PS, 6% CL (Zinser and Daum, 1995). For OMC + 0% CL and OMC + 17% CL, compensatory changes were made in the percentage of PC present in the lipid mixture. To examine lipid specificity, 20 or 40 mol% of the indicated phospholipid was mixed with 80 or 60 mol% PC, respectively. Headgroup-labeled lissamine rhodamine B phosphatidylethanolamine (Rd-PE) was added to all liposome mixtures in trace amounts.

Lipid mixtures were placed in a vacuum chamber overnight. The lipid films were rehydrated with 20 mM HEPES, pH 7.0, to a final lipid concentration of 2 mg/ml at room temperature for 1 h. Lipid mixtures were pipetted up and down to create a heterogeneous population of liposomes. Purified proteins and liposomes, as indicated, were added to gradient reaction buffer (GRB; 20 mM HEPES, pH 7.0, and 150 mM NaCl) for a total volume of 100 µl. This reaction was left at room temperature for 20 min. Four hundred microliters of 50% sucrose in GRB was added to the reaction mixture and added to the bottom of a 13 × 51 mm polycarbonate centrifuge tube (Beckman). The reaction plus sucrose mixture was overlaid with 1 ml 30% sucrose in GRB, 500 µl 10% sucrose in GRB, and 250 µl 0% sucrose in GRB for a total volume of 2.5 ml. Sucrose gradients were subjected to centrifugation in a Beckman SW55 rotor at 200,000 × *g* at 4°C for 2 h. Two 1.25 ml fractions were pipetted from the top, resulting in a top and bottom fraction. To monitor the efficiency of the liposome floats, the rhodamine fluorescence of each fraction was quantified using a SpectraMax M5 plate reader (Molecular Devices) with the excitation and emission monochromators set at 550 and 590 nm, respectively. In all cases, >85% of liposomes were observed in the top fraction. To quantify the fraction of protein that floated with the liposomes, equal volumes of top and bottom fractions were analyzed by SDS–PAGE followed by Western analysis using mouse monoclonal anti-T7 or anti-GFP (Invitrogen) for the primary antibody and goat anti-mouse immunoglobulin G (IgG) DyLight 680 (Pierce) or goat anti-rabbit IgG DyLight 800 (Thermo Fisher Scientific), respectively, for the secondary antibody. The immunoreactive bands were detected with the Odyssey Infrared Imaging System (Li-Cor Biosciences) and quantified using the accompanying software (Image Studio). For the high salt floats, the lipids were resuspended in 20 mM HEPES, pH 7.0, 450 mM NaCl, and the salt in the GRB was increased to 450 mM NaCl.

Cell extracts and Western blots

The indicated strains were grown to mid–log phase in yeast extract, peptone + 2% (wt/vol) dextrose (YPD) media. For Supplemental Figure S2, B and C, 0.5 nM estradiol and 0.05 nM estradiol were added, as indicated, to drive expression of GalS::*MMR1-yEGFP* and GalS::*MMR1ΔCC-yEGFP*, respectively. Cells (1.0 OD) were harvested, and whole cell extracts were prepared using a NaOH lysis and trichloroacetic acid (TCA) precipitation procedure. Each TCA pellet was resuspended in 50 µl MURB (100 mM MES, pH 7, 1% SDS, and 3 M urea). Whole cell extracts were analyzed by SDS–PAGE followed by Western analysis using anti-GFP (Invitrogen), anti-glucose-6-phosphate dehydrogenase (G-6-PDH; Sigma-Aldrich), or anti-phosphoglycerate kinase (PGK; Life Technologies) as the primary antibodies and goat anti-rabbit IgG DyLight 800 or goat anti-mouse IgG DyLight 680 (Thermo Fisher Scientific) as the secondary antibodies. The immunoreactive bands were detected with the Odyssey Infrared Imaging System (LI-COR Biosciences).

Immunoprecipitations

The indicated strains were grown to mid–log phase (~0.8 OD_{600}) in 50 ml YPD media. Cells were harvested, immediately frozen in liquid nitrogen, and stored at −80°C. Cell pellets were resuspended in 300 µl IP lysis buffer (IPLB; 20 mM HEPES-KOH, pH 7.4, 150 mM KOAc, 2 mM $Mg(Ac)_2$, 1 mM EGTA, 0.6 M sorbitol, Triton X-100) plus 1 mM DTT, 1X Protease Inhibitor Cocktail Set 1 (Millipore), and phosphatase inhibitors (60 mM β-glycerophosphate, 10 mM NaF, 1 mM sodium molybdate, 50 µM canthardin). Prechilled fine glass beads (0.5 mm glass beads; BioSpec cat # 11079105) were added to the lysates until only ~5 mm of lysate remained above the beads. Lysates were vortexed seven times at a setting of 9 for 1–1.5 min at 4°C with 1–1.5 min rest on ice between each vortexing session. Triton X (0.1%) was added to the lysates. Supernatants were removed from the glass beads by puncturing a hole in the bottom of each Eppendorf tube using a syringe needle (23 gauge), placing the tubes over empty Eppendorf tubes, and centrifuging the lysates into the new tubes at 0.9 × *g* for 30 s. The lysates in the new tubes were centrifuged at 17,000 × *g* for 30 min at 4°C to remove all large cell debris. Anti-FLAG or anti-GFP µMACS beads (25 µl; Miltenyi) were added to the supernatant, and the samples were placed on ice for 30 min. µMACS columns placed in magnetic holders were equilibrated with 250 µl IPLB + 0.1% Triton X-100 + PIC. The lysates were added to the equilibrated columns. Columns were washed with 800 µl IPLB + 0.1% Triton X-100 + PIC three times and with 500 µl IPLB, no detergent, no PIC twice. 1X MURB (25 µl) were added to the columns and incubated for 10 min at room temperature. An additional 25 µl 1X MURB was added to the column, and the 50 µl elution volume was collected. The cell lysate (5 µl) and immunoprecipitation elution fractions (15 µl) were analyzed by SDS–PAGE followed by Western analysis using anti-GFP (Invitrogen), anti-Myc (clone 9E10), or anti-FLAG (Sigma) as the primary antibodies and goat anti-rabbit IgG DyLight 800 or goat anti-mouse IgG DyLight 680 (Thermo Fisher Scientific) as the secondary antibodies. The immunoreactive bands were detected with the Odyssey Infrared Imaging System (LI-COR Biosciences) and quantified using the accompanying software (Image Studio).

Yeast two-hybrid analysis

PJ69-4A Δ*mmr1::NATNT2* and PJ69-4Alpha Δ*mmr1::NATNT2* were transformed with the indicated Gal4AD and Gal4BD fusions, respectively. PJ69-4A Δ*mmr1::NATNT2* cells harboring the indicated Gal4AD fusions were then mated with PJ69-4Alpha Δ*mmr1::NATNT2* cells harboring the indicated Gal4BD fusions. Diploids were selected on SC–LEU–TRP+DEX plates, and protein–protein interactions were assessed by growth on SC–LEU–TRP–ADE+DEX plates at 24°C.

ACKNOWLEDGMENTS

We thank members of the Lackner Lab, Suzanne Hoppins, Jennifer Brace, members of the Weiss Lab, and the Wignall-Lackner Cell Biology Group for suggestions and critical scientific discussions. We thank Yilan Wang and Jasmine Lucas for plasmid construction. We thank Lois Weisman for sharing the plasmid pCAD-C1 Myo2 CBD, Daniel Gottschling for sharing the plasmid pAGL, Stanley Fields and the Yeast Resource Center for sharing yeast two-hybrid strains, and Heather Pinkett for sharing the plasmid pWaldo-GFPd. We thank Jessica Hornick and instrumentation support from the Biological Imaging Facility at Northwestern University. W.C. is supported by National Institutes of Health (NIH) National Institute of General Medical Sciences (NIGMS) Training Grant no. T32GM008382. L.L.L. is supported by the NIH NIGMS Grant no. R01GM120303 and the Robert H. Lurie Comprehensive Cancer Center–The Lefkofsky Family Foundation/Liz and Eric Lefkofsky Innovation Research Award.

REFERENCES

Altmann K, Frank M, Neumann D, Jakobs S, Westermann B (2008). The class V myosin motor protein, Myo2, plays a major role in mitochondrial motility in *Saccharomyces cerevisiae*. J Cell Biol 181, 119–130.

Boldogh IR, Ramcharan SL, Yang HC, Pon LA (2004). A type V myosin (Myo2p) and a Rab-like G-protein (Ypt11p) are required for retention of newly inherited mitochondria in yeast cells during cell division. Mol Biol Cell 15, 3994–4002.

Cerveny KL, Studer SL, Jensen RE, Sesaki H (2007). Yeast mitochondrial division and distribution require the cortical num1 protein. Dev Cell 12, 363–375.

Chada SR, Hollenbeck PJ (2004). Nerve growth factor signaling regulates motility and docking of axonal mitochondria. Curr Biol 14, 1272–1276.

Chang SC, Heacock PN, Clancey CJ, Dowhan W (1998). The PEL1 gene (renamed PGS1) encodes the phosphatidylglycero-phosphate synthase of *Saccharomyces cerevisiae*. J Biol Chem 273, 9829–9836.

Chen S, Liu D, Finley RL, Greenberg ML (2010). Loss of mitochondrial DNA in the yeast cardiolipin synthase crd1 mutant leads to up-regulation of the protein kinase Swe1p that regulates the G2/M transition. J Biol Chem 285, 10397–10407.

Chernyakov I, Santiago-Tirado F, Bretscher A (2013). Active segregation of yeast mitochondria by Myo2 is essential and mediated by Mmr1 and Ypt11. Curr Biol 23, 1818–1824.

Connerth M, Tatsuta T, Haag M, Klecker T, Westermann B, Langer T (2012). Intramitochondrial transport of phosphatidic acid in yeast by a lipid transfer protein. Science 338, 815–818.

DeVay RM, Dominguez-Ramirez L, Lackner LL, Hoppins S, Stahlberg H, Nunnari J (2009). Coassembly of Mgm1 isoforms requires cardiolipin and mediates mitochondrial inner membrane fusion. J Cell Biol 186, 793–803.

Drew D, Lerch M, Kunji E, Slotboom DJ, de Gier JW (2006). Optimization of membrane protein overexpression and purification using GFP fusions. Nat Methods 3, 303–313.

Eves PT, Jin Y, Brunner M, Weisman LS (2012). Overlap of cargo binding sites on myosin V coordinates the inheritance of diverse cargoes. J Cell Biol 198, 69–85.

Fortsch J, Hummel E, Krist M, Westermann B (2011). The myosin-related motor protein Myo2 is an essential mediator of bud-directed mitochondrial movement in yeast. J Cell Biol 194, 473–488.

Frederick RL, Okamoto K, Shaw JM (2008). Multiple pathways influence mitochondrial inheritance in budding yeast. Genetics 178, 825–837.

Friedman JR, Lackner LL, West M, DiBenedetto JR, Nunnari J, Voeltz GK (2011). ER tubules mark sites of mitochondrial division. Science 334, 358–362.

Gohil VM, Thompson MN, Greenberg ML (2005). Synthetic lethal interaction of the mitochondrial phosphatidylethanolamine and cardiolipin biosynthetic pathways in *Saccharomyces cerevisiae*. J Biol Chem 280, 35410–35416.

Hoppins S, Collins SR, Cassidy-Stone A, Hummel E, Devay RM, Lackner LL, Westermann B, Schuldiner M, Weissman JS, Nunnari J (2011). A mitochondrial-focused genetic interaction map reveals a scaffold-like complex required for inner membrane organization in mitochondria. J Cell Biol 195, 323–340.

Hurd TR, Herrmann B, Sauerwald J, Sanny J, Grosch M, Lehmann R (2016). Long Oskar controls mitochondrial inheritance in *Drosophila melanogaster*. Dev Cell 39, 560–571.

Itoh T, Toh EA, Matsui Y (2004). Mmr1p is a mitochondrial factor for Myo2p-dependent inheritance of mitochondria in the budding yeast. EMBO J 23, 2520–2530.

Itoh T, Watabe A, Toh EA, Matsui Y (2002). Complex formation with Ypt11p, a rab-type small GTPase, is essential to facilitate the function of Myo2p, a class V myosin, in mitochondrial distribution in *Saccharomyces cerevisiae*. Mol Cell Biol 22, 7744–7757.

James P, Halladay J, Craig EA (1996). Genomic libraries and a host strain designed for highly efficient two-hybrid selection in yeast. Genetics 144, 1425–1436.

Janke C, Magiera MM, Rathfelder N, Taxis C, Reber S, Maekawa H, Moreno-Borchart A, Doenges G, Schwob E, Schiebel E, *et al*. (2004). A versatile toolbox for PCR-based tagging of yeast genes: new fluorescent proteins, more markers and promoter substitution cassettes. Yeast 21, 947–962.

Joshi AS, Thompson MN, Fei N, Hüttemann M, Greenberg ML (2012). Cardiolipin and mitochondrial phosphatidylethanolamine have overlapping functions in mitochondrial fusion in *Saccharomyces cerevisiae*. J Biol Chem 287, 17589–17597.

Katajisto P, Dohla J, Chaffer CL, Pentinmikko N, Marjanovic N, Iqbal S, Zoncu R, Chen W, Weinberg RA, Sabatini DM (2015). Stem cells. Asymmetric apportioning of aged mitochondria between daughter cells is required for stemness. Science 348, 340–343.

Klecker T, Scholz D, Fortsch J, Westermann B (2013). The yeast cell cortical protein Num1 integrates mitochondrial dynamics into cellular architecture. J Cell Sci 126, 2924–2930.

Kraft LM, Lackner LL (2017). Mitochondria-driven assembly of a cortical anchor for mitochondria and dynein. J Cell Biol 216, 3061–3071.

Kraft LM, Lackner LL (2018). Mitochondrial anchors: positioning mitochondria and more. Biochem Biophys Res Commun 500, 2–8.

Labbe K, Murley A, Nunnari J (2014). Determinants and functions of mitochondrial behavior. Annu Rev Cell Dev Biol 30, 357–391.

Lackner LL (2014). Shaping the dynamic mitochondrial network. BMC Biol 12, 35.

Lackner LL, Ping H, Graef M, Murley A, Nunnari J (2013). Endoplasmic reticulum-associated mitochondria-cortex tether functions in the distribution and inheritance of mitochondria. Proc Natl Acad Sci USA 110, E458–E467.

Lewandowska A, Macfarlane J, Shaw JM (2013). Mitochondrial association, protein phosphorylation, and degradation regulate the availability of the active Rab GTPase Ypt11 for mitochondrial inheritance. Mol Biol Cell 24, 1185–1195.

Lin MY, Sheng ZH (2015). Regulation of mitochondrial transport in neurons. Exp Cell Res 334, 35–44.

Longtine MS, McKenzie A 3rd, Demarini DJ, Shah NG, Wach A, Brachat A, Philippsen P, Pringle JR (1998). Additional modules for versatile and economical PCR-based gene deletion and modification in *Saccharomyces cerevisiae*. Yeast 14, 953–961.

Lwin KM, Li D, Bretscher A (2016). Kinesin-related Smy1 enhances the Rab-dependent association of myosin-V with secretory cargo. Mol Biol Cell 27, 2450–2462.

McFaline-Figueroa JR, Vevea J, Swayne TC, Zhou C, Liu C, Leung G, Boldogh IR, Pon LA (2011). Mitochondrial quality control during inheritance is associated with lifespan and mother-daughter age asymmetry in budding yeast. Aging Cell 10, 885–895.

Naylor K, Ingerman E, Okreglak V, Marino M, Hinshaw JE, Nunnari J (2006). Mdv1 interacts with assembled Dnm1 to promote mitochondrial division. J Biol Chem 281, 2177–2183.

O'Shea EK, Klemm JD, Kim PS, Alber T (1991). X-ray structure of the GCN4 leucine zipper, a two-stranded, parallel coiled coil. Science 254, 539–544.

Osman C, Voelker DR, Langer T (2011). Making heads or tails of phospholipids in mitochondria. J Cell Biol 192, 7–16.

Pashkova N, Catlett NL, Novak JL, Weisman LS (2005). A point mutation in the cargo-binding domain of myosin V affects its interaction with multiple cargoes. Eukaryot Cell 4, 787–798.

Pernice WM, Swayne TC, Boldogh IR, Pon LA (2017). Mitochondrial tethers and their impact on lifespan in budding yeast. Front Cell Dev Biol 5, 120.
Pernice WM, Vevea JD, Pon LA (2016). A role for Mfb1p in region-specific anchorage of high-functioning mitochondria and lifespan in *Saccharomyces cerevisiae*. Nat Commun 7, 10595.
Ping HA, Kraft LM, Chen W, Nilles AE, Lackner LL (2016). Num1 anchors mitochondria to the plasma membrane via two domains with different lipid binding specificities. J Cell Biol 213, 513–524.
Quintana A, Schwindling C, Wenning AS, Becherer U, Rettig J, Schwarz EC, Hoth M (2007). T cell activation requires mitochondrial translocation to the immunological synapse. Proc Natl Acad Sci USA 104, 14418–14423.
Schwarz TL (2013). Mitochondrial trafficking in neurons. Cold Spring Harb Perspect Biol 5, a011304.
Sheff MA, Thorn KS (2004). Optimized cassettes for fluorescent protein tagging in *Saccharomyces cerevisiae*. Yeast 21, 661–670.
Simbeni R, Pon L, Zinser E, Paltauf F, Daum G (1991). Mitochondrial membrane contact sites of yeast. Characterization of lipid components and possible involvement in intramitochondrial translocation of phospholipids. J Biol Chem 266, 10047–10049.
Simon VR, Karmon SL, Pon LA (1997). Mitochondrial inheritance: cell cycle and actin cable dependence of polarized mitochondrial movements in *Saccharomyces cerevisiae*. Cell Motil Cytoskeleton 37, 199–210.
Swaney DL, Beltrao P, Starita L, Guo A, Rush J, Fields S, Krogan NJ, Villen J (2013). Global analysis of phosphorylation and ubiquitylation cross-talk in protein degradation. Nat Methods 10, 676–682.
Swayne TC, Zhou C, Boldogh IR, Charalel JK, McFaline-Figueroa JR, Thoms S, Yang C, Leung G, McInnes J, Erdmann R, *et al*. (2011). Role for cER and Mmr1p in anchorage of mitochondria at sites of polarized surface growth in budding yeast. Curr Biol 21, 1994–1999.
Tang X, Germain BS, Lee WL (2012). A novel patch assembly domain in Num1 mediates dynein anchoring at the cortex during spindle positioning. J Cell Biol 196, 743–756.
van den Brink-van der Laan E, Killian JA, de Kruijff B (2004). Nonbilayer lipids affect peripheral and integral membrane proteins via changes in the lateral pressure profile. Biochim Biophys Acta 1666, 275–288.
Veatch JR, McMurray MA, Nelson ZW, Gottschling DE (2009). Mitochondrial dysfunction leads to nuclear genome instability via an iron-sulfur cluster defect. Cell 137, 1247–1258.
Zinser E, Daum G (1995). Isolation and biochemical characterization of organelles from the yeast, *Saccharomyces cerevisiae*. Yeast 11, 493–536.